

Optical counterpart of HLX-1 during the 2010 outburst³

R. Soria^{1*}, P. J. Hakala², G. K. T. Hau³, J. C. Gladstone⁴, A. K. H. Kong⁵

¹*International Centre for Radio Astronomy Research, Curtin University, GPO Box U1987, Perth, WA 6845, Australia*

²*Finnish Centre for Astronomy with ESO (FINCA), Väisäläntie 20, University of Turku, FIN-21500 Piikkiö, Finland*

³*European Southern Observatory, Alonso de Córdova 3107, Santiago, Chile*

⁴*Department of Physics, University of Alberta, Edmonton, Alberta, T6G 2C7, Canada*

⁵*Institute of Astronomy and Department of Physics, National Tsing Hua University, Hsinchu 30013, Taiwan*

Accepted Received ...; in original form ...

ABSTRACT

We studied the optical counterpart of the intermediate-mass black hole candidate HLX-1 in ESO 243-49. We used a set of Very Large Telescope imaging observations from 2010 November, integrated by *Swift* X-ray data from the same epoch. We measured standard Vega brightnesses $U = 23.89 \pm 0.18$ mag, $B = 25.19 \pm 0.30$ mag, $V = 24.79 \pm 0.34$ mag and $R = 24.71 \pm 0.40$ mag. Therefore, the source was ≈ 1 mag fainter in each band than in a set of *Hubble Space Telescope* images taken a couple of months earlier, when the X-ray flux was a factor of 2 higher. We conclude that during the 2010 September observations, the optical counterpart was dominated by emission from an irradiated disk (which responds to the varying X-ray luminosity), rather than by a star cluster around the black hole (which would not change). We modelled the Comptonized, irradiated X-ray spectrum of the disk, and found that the optical luminosity and colours in the 2010 November data are still consistent with emission from the irradiated disk, with a characteristic outer radius $r_{\text{out}} \approx 2800 r_{\text{in}} \sim 10^{13}$ cm and a reprocessing fraction $\approx 2 \times 10^{-3}$. The optical colours are also consistent with a stellar population with age $\lesssim 6$ Myr (at solar metallicity) and mass $\approx 10^4 M_{\odot}$; this is only an upper limit to the mass, if there is also a significant contribution from an irradiated disk. We strongly rule out the presence of a young super-star-cluster, which would be too bright. An old globular cluster might be associated with HLX-1, as long as its mass $\lesssim 2 \times 10^6 M_{\odot}$ for an age of 10 Gyr, but it cannot significantly contribute to the observed very blue and variable optical/UV emission.

Key words: accretion, accretion discs – X-rays: individual: HLX-1 – black hole physics.

1 INTRODUCTION

The point-like X-ray source 2XMM J011028.1–460421 (henceforth, HLX-1 for simplicity) is the strongest intermediate-mass black hole (IMBH) candidate known to date (Farrell et al. 2009; Davis et al. 2011; Servillat et al. 2011). It is seen in the sky at a distance of $\approx 8''$ from the nucleus of the S0 galaxy ESO 243-49 (redshift $z = 0.0224$, luminosity distance ≈ 95 Mpc, distance modulus ≈ 34.89 mag; at this distance, $1'' \approx 460$ pc). Its X-ray luminosity and spectral variability (Farrell et al. 2009; Godet et al. 2009; Servillat et al. 2011) are consistent with high and low states of an accreting BH. It shows recurrent outbursts every ≈ 370 d (seen in 2009 August, 2010 August, 2011 August),

due either to some kind of disk instability, or to a periodic enhancement of the accretion rate.

HLX-1 has an optical counterpart (Soria et al. 2010), with H α emission at a redshift consistent with that of ESO 243-49 (Wiersema et al. 2010), which strongly suggests a true physical association. Henceforth, we will assume that HLX-1 and ESO 243-49 are located at the same luminosity distance. The peak X-ray luminosity of HLX1 is $\approx 10^{42}$ erg s $^{-1}$, three orders of magnitude higher than typical stellar-mass X-ray binaries, and one order of magnitude higher than the most luminous ultraluminous X-ray sources (ULXs) found to-date. The BH mass required to be consistent with the Eddington limit is $\sim 10^4 M_{\odot}$, and a similar value is obtained from spectral modelling of the thermal X-ray component, which is consistent with emission from an accretion disk (Farrell et al. 2009; Davis et al. 2011; Servillat et al. 2011).

One of the most intriguing unsolved questions about

* E-mail: roberto.soria@icrar.org (RS); pahakala@utu.fi (PJH); ghau@eso.org (GKTH); jgladsto@ualberta.ca (JCG); akong@phys.nthu.edu.tw (AKHK).

HLX-1 is where it came from. There are no other luminous X-ray sources in ESO 243-49, in the range $\sim 10^{39}$ – 10^{41} erg s $^{-1}$; in fact, S0 galaxies do not generally contain extreme ULXs, which are more frequently found in spiral, irregular or interacting galaxies, with recent star formation (Swartz et al. 2004; Walton et al. 2011). For example, ULXs as luminous as $\approx 10^{41}$ erg s $^{-1}$ have been seen in the Cartwheel galaxy (Pizzolato et al. 2010), representing the upper end of a rich population of luminous X-ray sources, probably high-mass X-ray binaries. Instead, HLX1 appears to be an odd case within ESO 243-49.

Moreover, if the BH mass estimates are correct, HLX-1 is way too massive to have been formed from any stellar evolution process. Two conservative scenarios are that HLX-1 may be: a) the nuclear BH of a disrupted dwarf satellite galaxy, accreted by ESO 243-49 (King & Dehnen 2005); or, b) an IMBH formed inside a massive star cluster, perhaps via stellar coalescence and mergers (Portegies Zwart & McMillan 2002; Freitag et al. 2006). The location of HLX-1 outside the disk plane of ESO 243-49 is consistent with both scenarios—in fact, massive globular clusters such as ω Cen in the Milky Way may themselves be the remnants of nucleated dwarf galaxies (Bekki & Freeman 2003). IMBHs in massive star clusters, or floating in the outskirts of galaxies after minor mergers (O’Leary & Loeb 2009), have been predicted from theoretical arguments, or speculatively inferred from dynamical modelling (Gebhardt et al. 2005; Lützgendorf et al. 2011), but their existence is far from proven (van der Marel & Anderson 2010) and they have never been confirmed directly as luminous, accreting sources. Measuring the luminosity and colours of the optical counterpart, and their long-term variability, can help us test those scenarios. The optical emission may come from: the outer regions of the BH accretion disk; a star cluster around the BH; a single, massive and strongly irradiated donor star; a combination of all three. If the optical counterpart is dominated by a star cluster, we want to constrain its mass and age, which may give us a clue on the IMBH formation process.

In the rest of this paper, we present the results of our optical photometric study with the European Southern Observatory (ESO)’s Very Large Telescope (VLT). We use the optical and X-ray luminosities and colours to model the spectral energy distribution, and discuss the most likely scenarios for the optical emission. We also compare the optical brightness in our VLT images with the brightness measured in the *Hubble Space Telescope* (*HST*) observations of Farrell et al. (2011), taken when the X-ray luminosity of the source was higher.

2 VLT OBSERVATIONS

We observed HLX-1 with the Visible MultiObject Spectrograph (VIMOS) mounted on the Nasmyth focus B of UT3 Melipal, one of the four 8-m VLT telescopes at Cerro Paranal. We took three images in each of the *UBVRI* filters. Our observations were carried out in service mode, and were split between the night of 2010 November 7 (all *U*, *V* and *I*, and two out of three *B* observations) and 2010 November 26 (the last *B* and all *R* observations). All observations were

Date	Filter	MJD _{start}	Exp time
2010-11-07	U	55508.127	1560 s
	V	55508.147	375 s
	V	55508.152	375 s
	V	55508.157	375 s
	U	55508.164	1350 s
	U	55508.180	1350 s
	I	55508.198	165 s
	I	55508.201	165 s
	I	55508.203	165 s
	B	55508.208	560 s
	B	55508.215	560 s
2010-11-26	B	55527.139	560 s
	R	55527.148	285 s
	R	55527.152	285 s
	R	55527.156	285 s

Table 1. Log of our VLT VIMOS imaging observations.

taken in photometric conditions with an airmass $\lesssim 1.2$ and typical seeing $\approx 0''.7$ – $0''.8$. Standard fields were observed on each night. See Table 1 for a more detailed log of our observations.

The total exposure time was 4260 s in *U*, 1680 s in *B*, 1125 s in *V*, 855 s in *R* and 495 s in *I*. In all observations, HLX-1 was located approximately at the same position in Quadrant 1 of the VIMOS field. We used a standard dithering pattern for the three observations in each filter, to correct for pixel-to-pixel variations. For each filter, the three images were median-combined, and standard calibration procedures (cosmic ray filtering, bias subtraction, flat fielding) were applied through the ESO pipeline. In this paper, we focus on the Q1 imaging data, although we also extracted and analysed the data in the other three VIMOS chips, which cover a significant fraction of the Abell cluster 2877. We used SExtractor (Bertin & Arnout 1996) to build a catalogue of detected objects for each of the five median-combined images. We then used SCAMP and SWarp (Bertin et al. 2002; Bertin 2006) to read the SExtractor catalogues, compute astrometric solutions, and align the images in the various filters.

To convert from count rates to standard magnitudes (Vegamag) and fluxes at the top of the atmosphere, we used the standard relation

$$\text{Mag} = -2.5 \log (\text{Flux} [e^-/\text{s}]) + C_1 \text{Col} - C_2 \text{Airmass} + \text{ZP},$$

where C_1 is the colour coefficient suitable for a particular band, C_2 is the extinction coefficient, and ZP is the zero-point (different for each filter, in the Vegamag system). We used a gain of $1.76e^-/\text{ADU}$ to convert from directly measured fluxes in ADUs/s to fluxes in e^-/s . Zeropoints for our two nights were obtained from the pipeline-calibrated data files, and we also checked that they were consistent with the average values over the second semester of 2010, as listed on the ESO VIMOS quality control website¹. Average colour and extinction coefficients were obtained from the same website (summarized in Table 2). Not enough standard fields were observed in the two nights to permit us to determine

¹ www.eso.org/observing/dfo/quality/VIMOS/qc/zeropoints.html

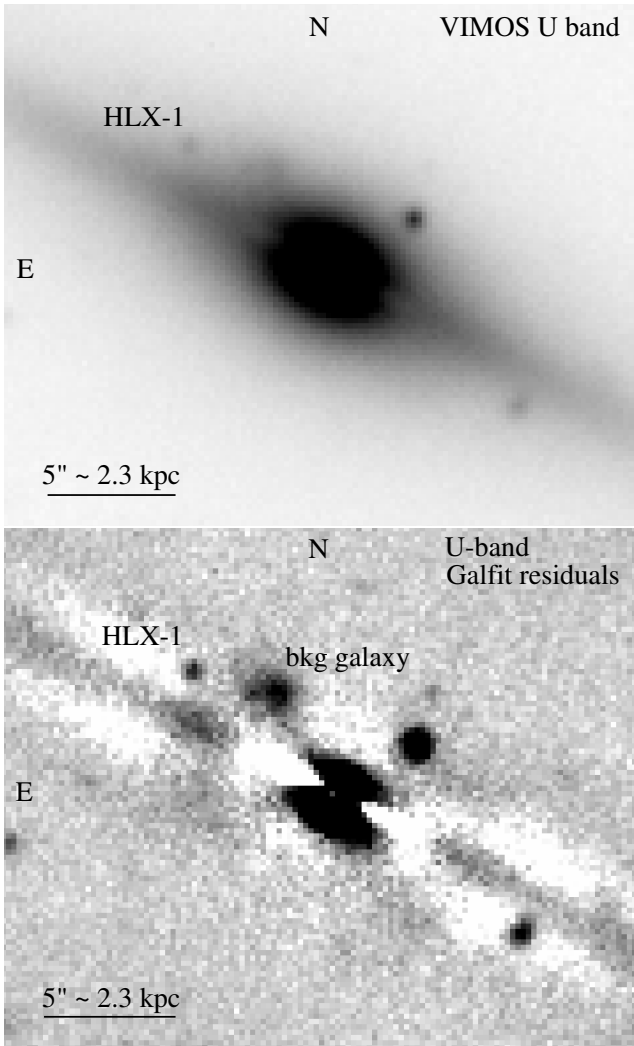


Figure 1. Top panel: combined U-band image from VLT VIMOS, observed on 2010 November 7; in the U-band, HLX-1 is marginally visible by eye before background subtraction. Bottom panel: an example of our efforts to model ESO 243-49 with several GALFIT components (see text).

the extinction coefficients on those specific nights; however, the error introduced by taking average colour and extinction coefficients is negligible compared with other sources of error. Finally, we need to correct for line-of-sight Galactic extinction in the direction of ESO 243-49, and any additional extinction intrinsic to the optical counterpart of HLX-1, in order to determine its true luminosity and colours. We will discuss this in Section 4.

3 OPTICAL DATA ANALYSIS AND RESULTS

HLX-1 is clearly detected in emission as a point-like source (Figure 1), coincident with the *Chandra* position and with the location of the optical counterpart identified from our *Magellan* images last year (Soria et al. 2010). In order to estimate its optical flux more accurately, first we had to model and remove the contribution of the host galaxy, that

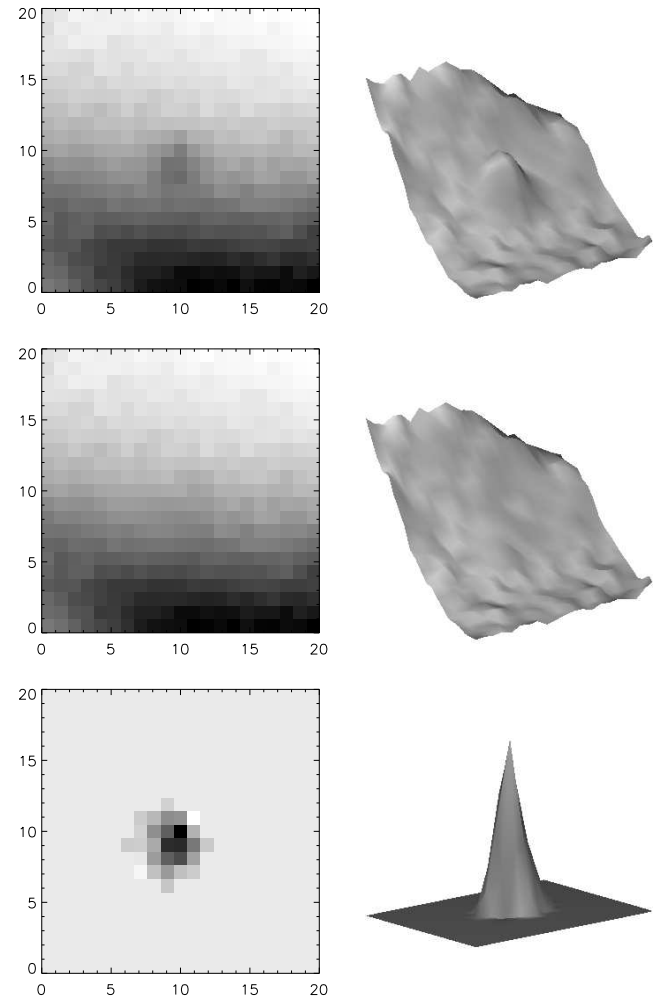


Figure 2. Top row: the subsection of the VLT VIMOS U-band image around HLX-1. Middle row: our best-fitting thin-plate spline local background model. Bottom row: the background-model-subtracted U-band image used for determining the optical brightness. In the left column, axis units are VIMOS pixels (North is up, East is left), with 1 pixel $\approx 0''.2$. In the right column, we display the same regions in 3-D format (North at the bottom, East to the right).

dominates the background emission particularly at redder colours. To do this, we tried two alternative techniques.

First, we tried modelling the galaxy light profile with GALFIT (Peng et al. 2002, 2010), and use the residuals to estimate the emission from HLX-1. The galaxy profile is quite complex; we tried fitting it with a combination of a Sérsic profile plus exponential disk plus edge-on disk plus disky/boxy profile, and a dust mask. However, the narrow dust lane across the disk plane creates artifacts and ripples that badly affect the wings of the HLX-1 point spread function (PSF) and the determination of the background level in the surrounding region; much higher spatial resolution from *HST* imaging (Farrell et al. 2011) is probably needed for this kind of modelling. Nonetheless, at least for the U and B bands, for which the galaxy halo contribution is less important, the GALFIT residuals do show HLX-1 as a point-like emission source and the background sub-

Filter	Zeropoint	Colour correction	Extinction coefficient	Mean airmass
U	26.09 ± 0.11	$(0.077 \pm 0.014) \times (U - B)$	0.38 ± 0.04	1.11
B	28.19 ± 0.02	$(-0.056 \pm 0.005) \times (B - V)$	0.24 ± 0.01	1.21
V	27.87 ± 0.02	$(-0.014 \pm 0.004) \times (B - V)$	0.12 ± 0.01	1.10
R	28.04 ± 0.05	$(-0.102 \pm 0.008) \times (V - R)$	0.08 ± 0.01	1.20
I	27.64 ± 0.04	$(0.049 \pm 0.006) \times (V - I)$	0.04 ± 0.02	1.19

Table 2. VIMOS Q1 zeropoints, colour coefficients, extinction coefficients and mean air masses used to convert from count rates to magnitudes.

traction is manageable. About $3''$ west of HLX-1, there is an extended, very blue source, probably a background star-forming galaxy (Farrell et al. 2011). This extended source is mostly responsible for the enhanced, asymmetric near-UV emission measured by Soria et al. (2010) in the north-east quadrant of ESO 243-49. After extensive tests, we concluded that the GALFIT method applied to our VLT data provides accurate results for the U and B bands, but the background-subtraction error is too large for the other bands. We used a 3-pixel source extraction region, a background annulus between 5 and 9 pixels, and applied suitable aperture corrections for the two bands (based on the PSF of isolated stars) to obtain the net count rates within an infinite aperture. We converted them to apparent magnitudes as outlined above. We obtained $U = 23.84 \pm 0.20$ mag and $B = 25.35 \pm 0.30$ mag.

We then used the following, more accurate technique. We excluded a circle of 5-pixel radius around the target and fitted a thin plate spline solution to the surrounding 21×21 (pixel)² area. This was done with the IDL routine *min.curve.surf*. This solution effectively follows the background exactly outside the exclusion zone, and provides a smooth solution for the background inside the exclusion zone (Figure 2). The main caveat of this technique is that the estimated background within the exclusion zone is affected by the values right outside the edge of the exclusion zone; in other words, if the exclusion circle is too small, the background inside it is overestimated, owing to the wings of HLX-1’s PSF extending right outside the exclusion circle. On the other hand, if the exclusion circle is too large, the fitting routine does not always provide smooth enough solutions through the whole aperture. After experimenting with several source and background region sizes, we decided to use an exclusion zone radius of 5 pixels and aperture radius of 3 pixels, from which we determined the net count rates (subsequently corrected to infinite aperture, with aperture corrections individually determined for each band). We estimated that the fraction of source counts in the PSF wings, falling in the background region, outside the 5-pixels exclusion radius, is between 5 and 10 per cent across the various filters; this is negligible compared to the number of background counts, and does not significantly affect the spline fitting or contribute to the error budget. We used zeropoint, colour-correction coefficients and extinction coefficients as before, to convert our results from count rates to standard (Vegamag) magnitudes, and then to AB magnitudes and flux densities (Table 3). We estimated the errors using a Monte Carlo method: we created synthetic data (1000 sets) based on the background model and the mea-

sured source count rates. Modelling the simulated data in the same way as the real data, we obtained the photometric errors quoted in Table 3. In summary, our final result is that $U = 23.89 \pm 0.18$ mag, $B = 25.19 \pm 0.30$ mag, $V = 24.79 \pm 0.34$ mag, $R = 24.71 \pm 0.40$ mag.

HLX-1 was not detected in the I band. This was not surprising, given the shorter exposure time and larger unresolved galactic contribution. We used a Monte Carlo technique to estimate the upper limits for the I band flux, in the following manner: we took the fitted I band background and added a fake point-like source of increasing brightness, in order to see how bright a source could be “hidden” for a given fitted background level and measured count rate in the source extraction region. We found that the 2σ and 3σ upper limits in the I band are $I > 25.8$ mag and $I > 24.4$ mag, respectively (Vegamag).

After we had completed our photometry study of the VLT data, the set of *HST* images obtained and studied by (Farrell et al. 2011) became available in the public archive. We used them to re-examine our source extraction techniques, checking that there were no other point-like sources in the regions we chose for background model fitting, and testing whether HLX-1 would still be detectable when blurred to VLT resolution. We show (Figure 3) that our choice of background regions are indeed suitable. While HLX-1 remains easily detectable in the F390W and F555W even after smoothing to lower resolutions, regardless of the choice of region for background fitting, re-detection of the source in the PSF-matched F775W image (the closest match available to the I band) depends strongly on background location and modelling, which introduces other sources of systematic error. Moreover, the source was ≈ 1 mag brighter in every band in the *HST* observations (Section 5.1). If that applies also to the I band, we would expect that $I \approx 25.5$ mag in the VLT data; but we see from the *HST* F775W image that there are another two and possibly three faint sources (marked as “a”, “b”, “c” in the bottom panel of Figure 3) of comparable brightness in I (~ 25.5 – 26 mag), which may contaminate the background region. Such sources would make the background region brighter, and therefore we would oversubtract from the HLX-1 source counts². For these reasons, we list conservative non-detection upper limits to the I band. We stress that the other four bands with robust detections already provide the information needed for the main conclusions of our study.

² The same contaminating sources are also present in the other bands, but are a less significant problem because HLX-1 is brighter.

Filter	λ_{eff} (Å)	m (Vegamag)	m_{AB} (ABmag)	M_0 (Vegamag)	F_{λ}^{obs} (erg cm ⁻² s ⁻¹ Å ⁻¹)	F_{λ}^0 (erg cm ⁻² s ⁻¹ Å ⁻¹)	F_{λ}^1 (erg cm ⁻² s ⁻¹ Å ⁻¹)
U	3650	23.89 ± 0.18	24.67 ± 0.18	-11.07 ± 0.18	(11.1 ^{+2.1} _{-1.7}) × 10 ⁻¹⁹	(11.8 ^{+2.2} _{-1.8}) × 10 ⁻¹⁹	(14.5 ^{+2.6} _{-2.1}) × 10 ⁻¹⁹
B	4380	25.19 ± 0.30	24.99 ± 0.30	-9.76 ± 0.30	(5.7 ^{+1.9} _{-1.4}) × 10 ⁻¹⁹	(6.1 ^{+2.0} _{-1.5}) × 10 ⁻¹⁹	(7.1 ^{+2.4} _{-1.7}) × 10 ⁻¹⁹
V	5450	24.79 ± 0.34	24.81 ± 0.34	-10.14 ± 0.34	(4.4 ^{+1.6} _{-1.3}) × 10 ⁻¹⁹	(4.5 ^{+1.7} _{-1.3}) × 10 ⁻¹⁹	(5.2 ^{+1.9} _{-1.5}) × 10 ⁻¹⁹
R	6410	24.71 ± 0.40	24.87 ± 0.40	-10.22 ± 0.40	(3.0 ^{+1.4} _{-1.0}) × 10 ⁻¹⁹	(3.1 ^{+1.4} _{-1.0}) × 10 ⁻¹⁹	(3.4 ^{+1.6} _{-1.1}) × 10 ⁻¹⁹
I	7980	> 24.4	> 25.0	> -10.0	< 1.7 × 10 ⁻¹⁹	< 1.8 × 10 ⁻¹⁹	< 1.9 × 10 ⁻¹⁹

Table 3. Summary of observed and de-reddened magnitudes and flux densities for HLX-1 during our 2010 November observations. m and m_{AB} are the apparent magnitudes at the top of the atmosphere (Vegamag and ABmag units, respectively). M_0 is the intrinsic absolute magnitude, corrected for a line-of-sight Galactic extinction $A_V = 0.04$ mag ($E(B - V) = 0.013$ mag) and a distance modulus = 34.89 mag. F_{λ}^{obs} is the observed top-of-the-atmosphere flux density (*i.e.*, the flux density corresponding to m_{AB}). F_{λ}^0 is the flux density corrected for a line-of-sight Galactic extinction $A_V = 0.04$ mag (a likely lower limit to the total optical extinction). F_{λ}^1 is the flux density corrected for an extinction $A_V = 0.18$ mag (a likely upper limit to the total optical extinction). The upper limits to the (non-detected) I brightness and flux are at the 99% confidence level. The other error ranges are 1σ .

We converted from observed brightnesses in the Vegamag system to top-of-the-atmosphere flux densities using VIMOS transmission models available online³. The VIMOS U-band filter is moderately different (Nonino et al. 2009) from the Johnson U-band filter (Bessell 1990) used to define the standard photometric system, while the other VIMOS filters have standard passbands. We double-checked our results using standard Vegamag-to-ABmag conversion tools⁴. In all cases, we adopted a blackbody input spectrum at $T = 25,000$ K for the flux density conversion (Table 3), but we also calculated the flux densities in the case of a flat spectrum, a $T = 10,000$ K blackbody, and various stellar models from O to A type. The reason we adopted $T = 25,000$ K is that the source has blue U-B and U-V colours, and does not appear to have a Balmer absorption jump typical of cooler stellar atmospheres. Anyhow, in all bands except for B, the flux density at the effective wavelength of the filter (also known as pivot wavelength), for a given magnitude, is essentially independent of spectral shape, within $\sim 1\%$. There is a small dependence on spectral shape/stellar type for the B band, because the Balmer jump falls at the high-frequency end of that passband. This introduces a systematic error of $\approx \pm 15\%$ of the flux values listed for the B band in Table 3, which is in any case less than the photometric uncertainty in the measured brightness.

Finally, we corrected for the optical extinction, in order to determine the true emitted luminosity and colours. As a first approximation, we took the foreground extinction $E(B - V) = 0.013$ mag (corresponding to $A_V \approx 0.04$ mag) from (Schlegel et al. 1998). An alternative possibility is to take the maps of Galactic HI from Kalberla et al. (2005), and convert N_{H} to an optical extinction for example through the relation of Güver & Özel (2009), $N_{\text{H}} = (2.21 \pm 0.09) \times 10^{21} A_V$ (corresponding to $A_V \approx 0.08$ mag). There may be additional extinction components, intrinsic to ESO 243-49, and in the local environment of HLX-1. For the ESO 243-49 component, we note that the halo of an S0

galaxy dominated by stellar populations older than 1 Gyr is not expected to contain much gas and dust; indeed, it was found (Di Stefano et al. 2003) that the best-fitting column densities for the brightest X-ray sources in the Sombrero galaxy (an edge-on S0 galaxy similar to ESO 243-49) are consistent or only marginally higher than the Galactic line-of-sight value. Moreover, optical/X-ray studies of Galactic black hole transients (fed via Roche-lobe overflow, as is likely the case in HLX-1) have shown (Hynes 2005) that the measured optical extinction is always smaller or comparable to the value that would be inferred from the values of N_{H} fitted to the X-ray spectra. This is because the local gas that contributes to the X-ray absorption is mostly confined to the X-ray emitting region, and/or is too hot to include a dusty component, so it does not contribute to the optical/UV absorption. In the case of HLX-1, we found from the *Swift*/XRT spectra that the total N_{H} fitted to the X-ray source is consistent with the foreground value, or is at most twice that value (Table 4). This is the same result obtained by Servillat et al. (2011) (total $N_{\text{H}} = (3 \pm 1) \times 10^{20}$ cm⁻² in the thermal state), while Godet et al. (2009) adopt $N_{\text{H}} \approx 4 \times 10^{20}$ cm⁻². Since we argued that the X-ray absorption provides an upper limit to the optical extinction, $A_V \lesssim 0.18$ mag. In Table 3, we list the top-of-the-atmosphere fluxes, those corrected with $A_V = 0.04$ mag, and those for $A_V = 0.18$ mag. The difference is small enough that none of our conclusions depends on the precise value of the extinction.

4 X-RAY IRRADIATION

One of our main objectives is to determine what fraction of the optical luminosity is due to re-emission of intercepted X-ray photons. Thus, we have to monitor the X-ray luminosity during the epoch of our VLT observations, and compare it with X-ray and optical luminosities at other epochs. Fortunately, HLX-1 has been the target of more than 100 *Swift* X-ray Telescope (XRT) observations since 2008 October; see NASA's HEASARC data archive for a detailed logbook. We used the on-line XRT data product generator (Evans et al.

³ <http://www.eso.org/observing/etc>

⁴ http://www.stsci.edu/hst/nicmos/tools/conversion_form.html

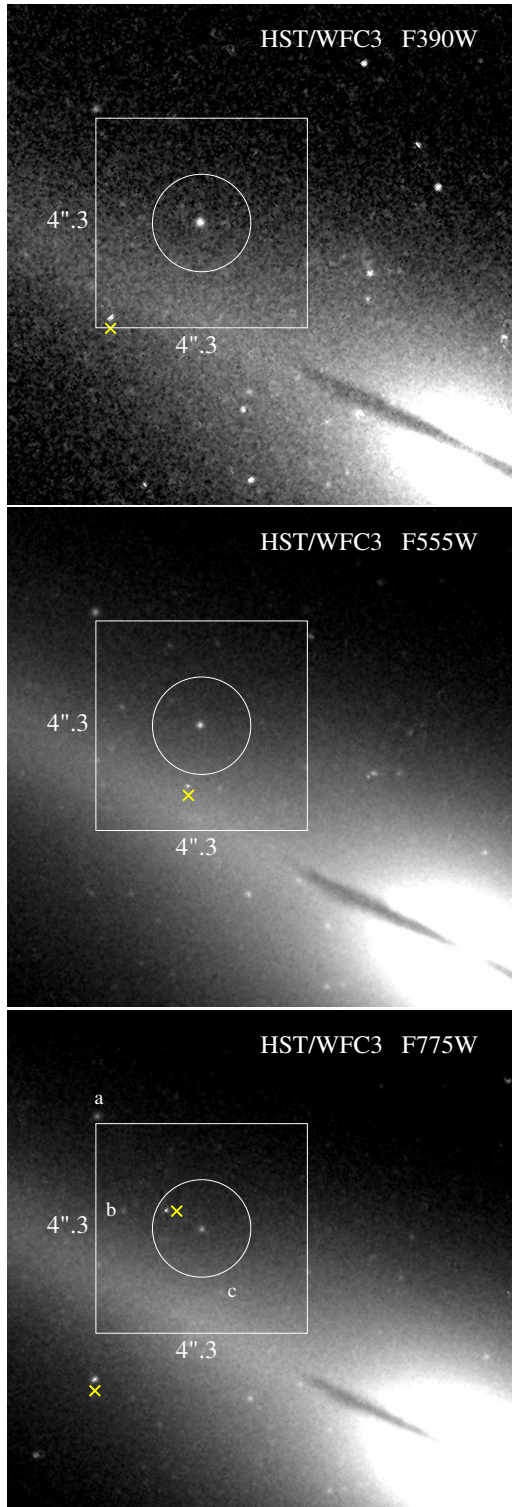


Figure 3. Top panel: *HST*/WFC3 image with the F390W filter, taken on 2010 September 23, with the outline of the region chosen for background modelling in our VLT study. North is up, East to the left. Middle panel: same as in the top panel, for the F555W filter image. Bottom panel: same, for the F775W filter image. In all panels, the box size is $\approx 4''.3 \times 4''.3$ and the radius of the exclusion circle is $\approx 1''$. Cosmic rays inside or near the extraction regions are marked with yellow crosses. The three faint sources marked with “a”, “b”, “c” in the F775W image may affect background subtraction in the VLT I band.

2007, 2009) to extract light curves and spectra (including background and ancillary response files); we selected grade 0–12 events. We downloaded the suitable spectral response file for single and double events in photon-counting mode from the latest *Swift* Calibration Database.

In 2010 November, HLX-1 was in the decline phase after the 2010 X-ray outburst. The X-ray luminosity did not change significantly between 2010 November 7 and 2010 November 26 (Figure 4), and the timescale for the exponential decay is much longer than 19 days. Thus, we can assume that the irradiation correction to the *R* band (observed on November 26) should not be significantly different from that affecting the optical bands on November 7. The individual *Swift*/XRT observations around the two epochs are too short to allow for meaningful spectral analysis. Therefore, to characterize the X-ray spectrum, we coadded all the observations in the middle part of the outburst decline, between 2010 September 30 and 2010 December 11, a period in which the X-ray source was almost on a plateau. Moreover, we coadded all *Swift*/XRT observations from 2008 October to 2011 August in which the 0.3–10 keV count rate was between 0.01 and 0.02 ct s⁻¹. We then fitted both co-added spectra with XSPEC version 12 (Arnaud 1996), using the Comptonized, irradiated disk model *diskir* (Gierliński et al. 2008).

An advantage of the *diskir* model over widely used two-component models such as *diskbb* plus *power-law* is that the Comptonized component is physically truncated at low energies, and the disk spectrum can easily be extrapolated to the optical bands, and compared with the flux from the optical counterpart. We fixed the fraction f_{in} of luminosity in the Compton tail that is thermalized in the inner disk to 0.1 (Gierliński et al. 2008). The other irradiation parameter in the model, f_{out} , is the fraction of bolometric flux that is thermalized in the outer disk. The value of f_{out} and of the outer disk radius r_{out} are essentially unconstrained when we fit the X-ray data, especially for a cool disk with peak temperature $\lesssim 0.2$ keV, but will become important for the optical extrapolation.

We find that the long- and short-baseline *Swift*/XRT spectra are essentially identical in shape and normalization (Figure 5). The exposure time for the long spectrum was 1.2×10^5 s; the exposure time for the short spectrum (which is simply a subset of the longer-baseline data) was 4.7×10^4 s. The best-fitting parameters for the long-baseline spectrum are listed in Table 4. This result is consistent with the expected spectral behaviour of HLX-1 at intermediate luminosities (Servillat et al. 2011), with a soft thermal component that is still dominant, and an emerging power-law that becomes harder during the decline. The emitted luminosity $L_{0.3-10\text{keV}} \approx 5.5 \times 10^{41}$ erg s⁻¹, a factor of 2 lower than at the outburst peak. The disk normalization implies an inner radius $r_{\text{in}} \approx 6 \times 10^4$ km (for an approximately face-on disk), indicative of a BH mass $\sim 10^4 M_{\odot}$ and consistent with previous X-ray studies (Davis et al. 2011; Servillat et al. 2011).

5 OPTICAL/X-RAY COMPARISON

After measuring the optical brightness in the VLT dataset, and modelling the temperature and luminosity of the X-ray-emitting accretion disk, we shall now discuss whether the

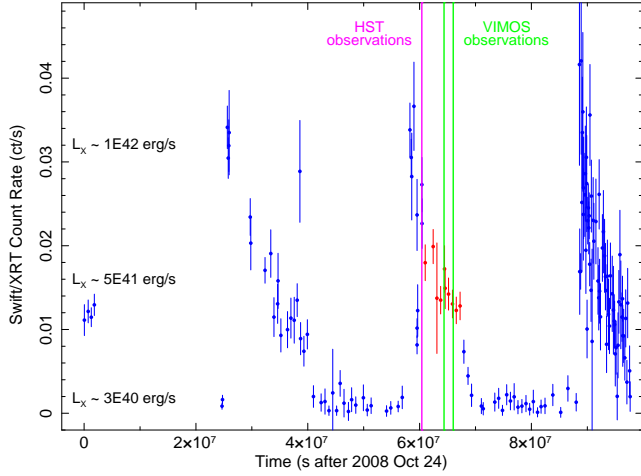


Figure 4. *Swift*/XRT lightcurve in the 0.3–10 keV band, between 2008 October 24 and 2011 November 28. The two epochs of our VLT observations are indicated by vertical green lines; the epoch of the *HST* observations is also plotted. We integrated to *Swift*/XRT spectrum from the epochs plotted in red, to determine the irradiation conditions around the time of our VLT observations.

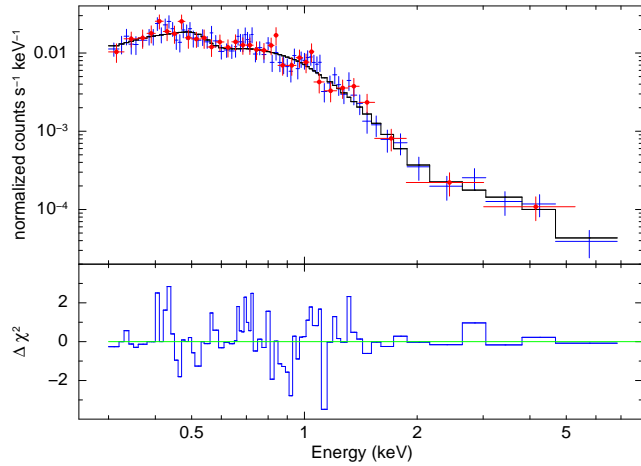


Figure 5. *Swift*/XRT spectrum modelled with the Comptonized, irradiated disk model *diskir* in XSPEC. The blue spectrum includes all the epochs when the XRT count rate was between 0.01 and 0.02 ct s⁻¹. The red datapoints are a subset of the blue datapoints, for the epochs plotted in red in Figure 4. The χ^2 residuals in the bottom panel refer to the long-baseline spectrum, which has better signal-to-noise and provides stronger constraints.

optical emission is more likely to come from the outer part of the irradiated disk, from a stellar population or from a single donor star. A comparison with the optical brightness in the *HST* observations (Farrell et al. 2011) provides a crucial test to distinguish between those models.

Parameter	Value
$N_{\text{H,Gal}}$	[2.0]
$N_{\text{H,int}}$	$0.8^{+2.4}_{-0.8}$
kT_{in}	$0.17^{+0.01}_{-0.05}$
Γ	$1.59^{+0.68}_{-0.34}$
kT_e	[100]
L_C/L_d	$0.60^{+4.33}_{-0.45}$
f_{in}	[0.1]
r_{irr}	[1.2]
f_{out}	$[2 \times 10^{-3}]$
$\log(r_{\text{out}}/r_{\text{in}})$	[3.45]
N_{disk}	$40.6^{+91.7}_{-13.5}$
$f_{0.3-10}$	$4.1^{+0.2}_{-0.2}$
$L_{0.3-10}$	$5.5^{+0.4}_{-0.6}$
χ^2_{ν}	0.83 (55.3/67)

Table 4. Best-fitting spectral parameters for the coadded *Swift*/XRT observations during intermediate-luminosity states. Units: $N_{\text{H,Gal}}$ and $N_{\text{H,int}}$ are in units of 10^{20} cm⁻²; kT_{in} and kT_e in keV; r_{irr} in units of the inner-disk radius r_{in} ; $f_{0.3-10}$ in 10^{-13} erg cm⁻² s⁻¹; $L_{0.3-10}$ in 10^{41} erg s⁻¹. The disk normalization $N_{\text{disk}} = [(r_{\text{in}}/\text{km}) / (D/10\text{kpc})]^2 \cos\theta$, where $\cos\theta$ is the viewing angle of the disk. Errors indicate the 90% confidence interval for each parameter of interest.

5.1 Optical decline between the *HST* and VLT observations

The X-ray luminosity, as determined from the *Swift*/XRT count rate and spectra, was a factor of ≈ 2 higher during the 2010 September 23 *HST* observations than during our VLT observations, taken at a later stage of the 2010 outburst decline. We showed (Table 3) that the optical/near-UV brightness of HLX-1 was ≈ 24.7 –25.0 mag (ABmag system) in our VLT data; in the *HST* observations, it was ≈ 23.8 –24.0 mag (Farrell et al. 2011)⁵. Although the VIMOS filter bands are slightly different from the *HST* bands, this discrepancy in flux density occurs in every band and cannot be explained with colour transformations; as we are referring to the top-of-the-atmosphere flux density, this is also independent of the different choices of line-of-sight and intrinsic extinction corrections. Interpolating the flux densities given by Farrell et al. (2011) across our observed bands, we determine that the VLT flux was fainter than during the *HST* observations, with 3σ significance in each of the U,B,V and I bands, and 2.5σ significance in R. Thus, we conclude that the source had significantly dimmed, by ≈ 1 mag, in the near-UV/optical/near-IR bands. To test possi-

⁵ We also independently checked that HLX-1 was significantly brighter in the *HST* images, by doing relative photometry with a dozen other sources detected in both fields.

ble further evidence of variability in the optical counterpart, we also re-examined our Magellan observations (Soria et al. 2010), taken a few days after the 2009 August outburst peak, when the X-ray flux was, again, a factor of 2 higher than in 2010 November. The Magellan R-band brightness $m_{\text{AB},R} \approx 24.0 \pm 0.3$ mag is ≈ 0.9 mag higher than in our 2010 VLT observations, with a 2σ significance. (The larger error in the Magellan V-band measurement, which we now re-estimate as $m_{\text{AB},V} \approx 24.5 \pm 0.5$ mag prevents firm conclusions on that band.)

On its own, our discovery of long-term optical variability correlated with the X-ray luminosity already rules out the possibility that the optical/UV counterpart was dominated by emission from an old globular cluster or a young super-star-cluster during the *HST* observations, as discussed in Farrell et al. (2011). Hence, we suggest that the dominant optical/UV contribution near the outburst peak was from an irradiated accretion disk. Any additional contribution from a (constant-luminosity) stellar population must be fainter than the luminosity determined from our VLT observations.

In fact, even in our VLT data, the accretion disk is likely to give a significant contribution to the optical/UV flux, as the X-ray luminosity was still 20 times higher than in the low state, and the soft X-ray flux was still dominated by (partly Comptonized) disk emission (Table 4). In the rest of this Section, we are going to discuss and constrain the possible contribution of disk and stellar populations in our VLT data.

5.2 Irradiated disk

The simplest scenario is a standard (Shakura & Sunyaev 1973) non-irradiated disk, with inner temperature and normalization derived from X-ray fitting (Table 4), extrapolated to an infinite radius (for practical purposes, $r_{\text{out}} = 10^5 r_{\text{in}}$). This is plotted as a solid black line in all panels of Figure 6; in those plots, X-ray absorption has been removed from the disk model, and the optical datapoints have been corrected for a line-of-sight reddening $E(B - V) = 0.013$ mag⁶. In the optical band, the predicted non-irradiated disk emission approximately reproduces the spectral slope between U and R but falls a factor of 3 below the observed brightnesses.

Clearly, irradiation of the outer disk is needed to increase the optical flux of the model without changing the X-ray luminosity. First, we assumed an irradiation fraction $f_{\text{out}} = 10^{-3}$ while keeping a large outer radius ($r_{\text{out}} = 10^5 r_{\text{in}}$). The predicted optical flux (solid green line in Figure 6) is now roughly consistent with the VLT data from U to R (although the U-V colour is too red), but is much too bright for the I band. As a general rule, the optical emission of a large irradiated disk is redder than the emission of a non-irradiated disk. However, our source is significantly bluer.

Truncating (or shading) the outer edge of the disk removes some of the red emission from the outer regions, and makes the optical slope steeper. We find that the optical data are well fitted (solid blue line in Figure 6) with emission from the same accretion disk seen in the X-ray band,

extending to $r_{\text{out}} \approx 2800 r_{\text{in}} \approx (1.7 \times 10^{13}) / \cos \theta$ cm, and with an intercepted and re-radiated fraction of X-ray photons $f_{\text{out}} \approx 2 \times 10^{-3}$, a very plausible value for irradiated disks in binary systems. Reprocessing fractions of \sim a few times 10^{-3} are suggested both by theoretical modelling (e.g., Vrtilik et al. 1990; de Jong et al. 1996; King & Ritter 1998; Dubus et al. 1999) and by observations of accretion disks in Galactic BHs (e.g., Hynes et al. 2002; Gierliński et al. 2009). In summary, considering that an irradiated disk was the dominant optical/UV emitter in 2010 September (Section 5.1), and that the X-ray flux from the inner disk was still relatively high in 2010 November, we take the irradiated disk scenario as the most likely interpretation also for the optical emission in our VLT data.

5.3 Stellar population

An alternative possibility is that most of the optical emission in the VLT data comes from a massive star cluster surrounding the BH. For example, this is what we expect if the IMBH was the nucleus of a recently accreted satellite dwarf, or was formed from core collapse in a massive star cluster. We ran instantaneous star formation simulations with STARBURST99 (Leitherer et al. 1999; Vázquez & Leitherer 2005) to determine the expected brightness and colours of star clusters of various masses and ages (we assumed solar metallicity for simplicity, and a Kroupa initial mass function). Here, we focus on a few representative cases.

We find that a young super-star-cluster (for example, the solid cyan line in the top panel of Figure 6 represents a cluster with $M = 10^6 M_{\odot}$ and age of 10 Myr) is inconsistent with the VLT optical data: it would have blue colours and small or no Balmer jump, consistent with the observed data, but would be much too bright. This rules out one of the scenarios presented in Farrell et al. (2011). A young star cluster with much lower mass can match the observed optical luminosity and colours; the solid cyan line in the bottom panel of Figure 6 represents a cluster with $M = 1.4 \times 10^4 M_{\odot}$ and age of 5 Myr. In fact, this is only an upper limit to the young cluster mass, if there is still a significant disk contribution (Section 5.2). A stellar population age $\lesssim 6$ Myr is required in order to match the optical colours, at solar metallicity—modulo the age-metallicity degeneracy⁷. However, the physical interpretation of this scenario is problematic. A $10^4 M_{\odot}$ cluster is too small to harbour an IMBH formed from runaway core collapse (Portegies Zwart & McMillan 2002; Freitag et al. 2006), especially one as massive as required for HLX-1 (Davis et al. 2011), similar to the mass of the cluster itself. Its very young age makes it unlikely that the cluster could be much more massive at birth. Moreover, the *HST* near-UV images show no other signs of ongoing or very recent, clustered star formation in the region surrounding HLX-1, which appears like a one-off object. For all these reasons, we conclude that the young-star-cluster scenario is much less likely than the irradiated disk scenario.

Old globular clusters are much fainter for a given stellar mass. A cluster with $M = 10^6 M_{\odot}$ and age of 1 Gyr would be

⁶ Using our upper limit $E(B - V) = 0.06$ mag does not change any of the arguments in this Section.

⁷ In simple terms, the age-metallicity degeneracy means that colours and luminosity are the same for a stellar population with half the metal abundance and three times the age (Worthey 1994).

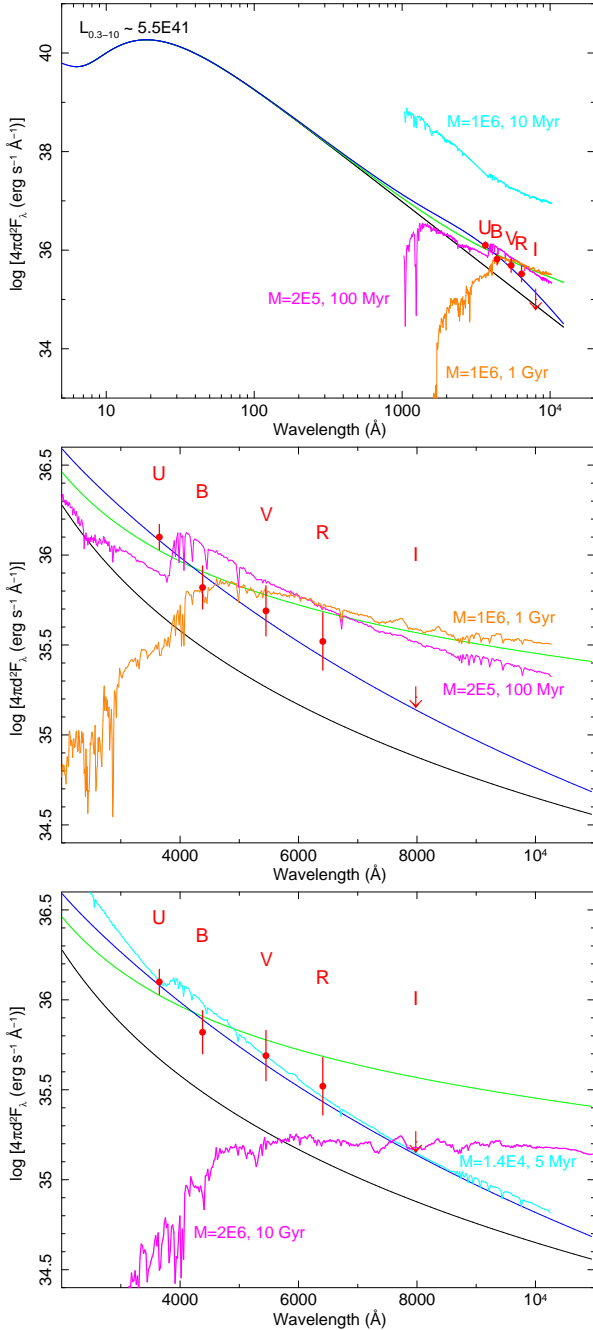


Figure 6. Top panel: optical/UV flux densities from our VLT data (plotted in red), compared with the model flux density predicted from various types of accretion disks and stellar populations. At high energies, the disk parameters are fixed from the fit to the *Swift*/XRT data. Black line: standard, non-irradiated disk spectrum; green line: irradiated disk; blue line: irradiated, truncated disk; cyan line: spectrum of a young, massive star cluster; magenta line: spectrum of an intermediate-age stellar population; orange line: spectrum of an old globular cluster. Middle panel: zoomed-in view in the optical/UV band, plotted in linear scale: the three disk spectra and the two old/intermediate-age stellar populations are as in the top panel. Bottom panel: the spectrum of a low-mass, very young stellar population (cyan line) fits the data as well as the irradiated, truncated disk model (blue line) but may not have a simple physical interpretation; an very old, massive globular cluster may also be associated with HLX-1, provided that its mass is $\lesssim 2 \times 10^6 M_{\odot}$ (magenta line).

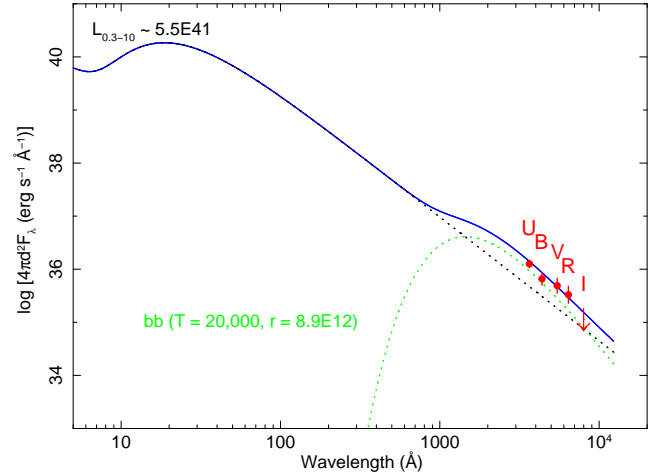


Figure 7. Optical/UV flux densities from our VLT data (plotted in red), compared with a model consisting of a standard non-irradiated disk (dotted blue line) plus a single blackbody with $T = 20,000$ K and characteristic size $\approx 8.9 \times 10^{12}$ cm $\approx 130R_{\odot}$ (dotted green line).

marginally consistent with the observed B, V, R brightnesses (solid orange line in Figure 6, middle panel), but totally inconsistent with the observed colour $U - B \approx -1.3$ mag, which is typical of OB stars, and with the upper limit to the I band. Intermediate-age (≈ 50 – 100 Myr) clusters with masses $\sim 10^5 M_{\odot}$ are a slightly better match to the B, V, R optical data but remain inconsistent with U and I (solid magenta line in Figure 6, middle panel). The strongest constraint against intermediate-age and old stellar populations comes from the apparent lack of a Balmer jump between B and U, in our VLT observations; this implies that Hydrogen is mostly ionized at the photosphere of the optical emitter. If the emitter is a stellar population, the lack of a Balmer jump alone strongly suggests an age $\lesssim 50$ Myr. We conclude that the optical counterpart of HLX-1 cannot be dominated by a massive old or intermediate-age globular cluster.

More complex and/or contrived theoretical scenarios can also be proposed. For example, the IMBH could be located in an old, faint globular cluster (perhaps the parent cluster that formed the IMBH via core collapse in earlier epochs) with an age > 1 Gyr and current mass \lesssim a few $\times 10^5 M_{\odot}$ (thus, satisfying the VLT luminosity constraints), which has recently undergone a new burst of star formation, that produced a $\sim 10^4 M_{\odot}$ young stellar population (including perhaps the donor star to the IMBH). Or, the blue optical emission may come entirely from the IMBH disk, inside an old globular cluster, and the mass donor may be an evolved low-mass star. For a globular cluster with an age of 10 Gyr, the upper mass limit consistent with the VLT data is $\approx 2 \times 10^6 M_{\odot}$ (Figure 6, bottom panel). Such an old cluster would dominate the near-IR emission but would give a negligible contribution to the optical/UV bands, compared with the irradiated disk and/or young stellar population. We do not have enough observational data at the moment to test such multiple-component scenarios. New observations of HLX-1 during a much lower X-ray state, and in the IR, will provide conclusive tests between the irradiated disk and

star cluster models, and may provide a more quantitative estimate or upper limit to the optical contribution of a stellar population around the BH.

Finally, we may want to consider the possibility that the optical emission comes from the surface of an individual donor star. The inferred absolute magnitude $M_V \sim M_B \sim -10$ mag is very high but not beyond the limit of existing stars, for example blue hypergiants and Luminous Blue Variables (LBVs). Stars in this luminosity range include Cyg OB2-304, the most luminous star known to-date in the Galaxy ($M_V = -10.6$ mag; Massey et al. 2001); η Carinae was also at $M_V \lesssim -10$ mag in the early 19th century, before the 1843 Great Eruption (Frew 2004).

As an extreme case, we modeled a standard non-irradiated disk (based on the X-ray parameters, as in Section 5.1) with an additional single-temperature blackbody component. We find that for $T_{\text{bb}} \approx 20,000$ K and a stellar radius $r_* \approx 8.9 \times 10^{12}$ cm $\approx 130R_\odot$, the resulting spectrum also matches the observed optical data (Figure 7) as well as the irradiated disk spectrum. We cannot distinguish between the two cases with the scant optical data at hand. What this means is that most of the optical emission may come from a region with characteristic size $\sim 10^{13}$ cm and characteristic temperature $\sim 20,000$ K: either the outer radius of the irradiated (part of the) disk, or the irradiated face of a large, massive donor star. A scenario where the optical luminosity is dominated by a single LBV or blue hypergiant donor star implies the presence of ellipsoidal variations, due to the tidally-distorted shape of the star, and orbital modulations, due to the variable fraction of the irradiated face of the star visible to us during the orbit. The single-donor scenario may perhaps explain the outburst period ≈ 370 d seen in the X-ray lightcurve (Lasota et al. 2011), if the orbit is elongated and Roche-lobe mass transfer occurs mostly at periastron, with the formation of a disk. However, it is very unlikely that the optical/UV counterpart is a single donor star, because there are no other similar objects or other evidence of exceptional star formation in the surrounding regions, within at least 1 kpc. Another issue to consider is that such massive stars are shrouded in dense winds, in apparent contrast with the low column density measured from the X-ray spectra; on the other hand, the wind may be completely ionized because of the X-ray emission from the BH. Deeper optical spectra of the optical counterpart may help test between those scenarios.

6 CONCLUSIONS

We observed the optical counterpart of HLX-1 with VLT VIMOS, in 2010 November, when the X-ray source was in an intermediate state, declining after the 2010 August outburst. We found the following brightness values in the standard Vegamag system: $U = 23.89 \pm 0.18$ mag; $B = 25.19 \pm 0.30$ mag; $V = 24.79 \pm 0.34$ mag; $R = 24.71 \pm 0.40$ mag. In the ABmag system, this corresponds to $m_{\text{AB},U} = 24.67 \pm 0.18$ mag, $m_{\text{AB},B} = 24.99 \pm 0.30$ mag, $m_{\text{AB},V} = 24.81 \pm 0.34$ mag, $m_{\text{AB},R} = 24.87 \pm 0.40$ mag. We do not detect the source in the I band ($m_{\text{AB},I} > 25.0$ mag); this was expected because the I band had the shortest exposure time and the largest galactic contamination.

We found that the optical/UV brightnesses in every

band are ≈ 1 mag fainter than in the *HST* observations from 2010 September, at a time when the X-ray flux was a factor of 2 higher. This rules out the scenario (Farrell et al. 2011) that the optical source seen in the *HST* observations was dominated by a massive star cluster, because in that case its brightness would not have changed. It strongly suggests that the optical counterpart was dominated by an irradiated accretion disk.

From the VLT data alone, we cannot tell whether the optical emission was still dominated by an irradiated disk, or by a stellar population: optical observations at even lower X-ray flux levels will test these alternatives. We can, however, constrain the maximum stellar mass and age of the stellar population that can be consistent with the observed VLT luminosities and colours. We found that they are consistent with a young stellar population of mass $\sim 10^4 M_\odot$ and age $\lesssim 10$ Myr. This immediately rules out a young super-star-cluster, which would have similar blue colours and lack of a Balmer jump, but would be much too luminous. If there is an old globular cluster around HLX-1, as previously speculated (Soria et al. 2010), it may dominate the near-IR bands, but it cannot give a significant contribution to the observed optical/UV flux discussed in this work. We estimate that a 10-Gyr-old globular cluster must have a mass $\lesssim 2 \times 10^6 M_\odot$ to be consistent with the VLT data. By comparison with the current models and observational mass limits on IMBH candidates in old globular clusters (Table 1 in van der Marel & Anderson 2010), we argue that a host cluster mass $\approx 2 \times 10^6 M_\odot$ may be just high enough at least to allow for the possibility of a central IMBH with a mass $\approx 10^4 M_\odot$, as suggested by X-ray modelling (Servillat et al. 2011; Davis et al. 2011).

In conclusion, we attribute most of the optical/UV emission to an irradiated disk, as the simplest scenario consistent with all the data at hand. The more complex scenario of a very old globular cluster with a small burst of recent star formation is also acceptable, but requires more observational data to be tested. We modelled the X-ray spectrum around the time of the VLT observations (when $L_{0.3-10} \approx 5.5 \times 10^{41}$ erg s $^{-1}$), and during epochs of similar levels of X-ray luminosity in previous years. We showed that an irradiated disk can explain the observed optical luminosity and colours, with a plausible reprocessing fraction $\approx 2 \times 10^{-3}$, typical of irradiated disks in X-ray binaries. Regardless of any details on disk structure and irradiation, if the optical emission is thermal, during the VLT observations it comes from a region with characteristic size $\sim 10^{13}$ cm and characteristic temperature $\approx 20,000$ K; this could be the size and temperature of the irradiated outer disk.

ACKNOWLEDGMENTS

We thank Chris Done, Sean Farrell, Paul Kuin, Kip Kuntz, Manfred Pakull, Ivo Saviane, Curtis Saxton, Kinwah Wu for illuminating discussions. In particular, we are very grateful to Sean Farrell and Mat Servillat for sharing and discussing their *HST* results in advance of publications. We thank the anonymous referee for a number of useful suggestions and constructive criticism. RS acknowledges support from a Curtin University Senior Research Fellowship, and hospitality at the ESO headquarters in Santiago (Chile),

at the Mullard Space Science Laboratory (UK) and at the University of Sydney (Australia) during part of this work. JCG acknowledges support from the Avadh Bhatia Fellowship and Alberta Ingenuity.

REFERENCES

- Arnaud K.A., 1996, ASP Conference Series, Vol. 101, Astronomical Data Analysis Software and Systems V., Astron. Soc. Pac., San Francisco, G. Jacoby and J. Barnes, eds., p. 17
- Bekki K., Freeman K.C., 2003, MNRAS, 346, L11
- Bertin E., 2006, Automatic Astrometric and Photometric Calibration with SCAMP, ASP Conference Series, Vol. 351, C. Gabriel, C. Arviset, D. Ponz, and E. Solano, eds., p. 112
- Bertin E., Arnouts S., 1996, A&AS, 317, 393
- Bertin E., Mellier Y., Radovich M., Missonnier G., Didelon P., Morin, B., 2002, ASP Conference Series, Vol. 281, D.A. Bohlender, D. Durand, and T.H. Handley, eds., p. 228
- Bessell M.S., 1990, PASP, 102, 1181
- Davis S.W., Narayan R., Zhu Y., Barret D., Farrell S.A., Godet O., Servillat M., Webb N.A., 2011, ApJ, 734, 111
- de Jong J.A., van Paradijs J., Augusteijn T., 1996, A&A, 314, 484
- Di Stefano R., Kong A.K.H., VanDalsen M.L., Harris W.E., Murray S.S., Delain K.M. 2003, ApJ, 599, 1067
- Dubus G., Lasota J.-P., Hameury J.-M., Charles P., 1999, MNRAS, 303, 139
- Evans P.A., et al., 2007, A&A, 469, 379
- Evans P.A., et al., 2009, MNRAS, 397, 1177
- Farrell S.A., Webb N.A., Barret D., Godet O., Rodrigues J.M., 2009, Nature, 460, 73
- Farrell S.A., et al., 2011, ApJ, submitted (arXiv:1110.6510)
- Freitag M., Gürkan M.A., Rasio, F.A., 2006, MNRAS, 368, 141
- Frew D.J., 2004, JAD, 10, 6
- Gebhardt K., Rich R.M., Ho L.C., 2005, ApJ, 634, 1093
- Gierliński M., Done C., Page K., 2008, MNRAS, 388, 753
- Gierliński M., Done C., Page K., 2008, MNRAS, 392, 1106
- Godet O., Barret D., Webb N.A., Farrell S.A., Gehrels, N., 2009, ApJ, 705, L109
- Güver T., Özel F., 2009, MNRAS, 400, 2050
- Hynes R.I., Haswell C.A., Chaty S., Shrader C.R., Cui W. 2002, MNRAS, 331, 169
- Hynes R., 2005, ApJ, 623, 1026
- Kalberla P.M.W., Burton W.B., Hartmann D., Arnal E.M., Bajaja E., Morras R., Pöppel W.G.L., 2005, A&A, 440, 775
- King A.R., Dehnen W., 2005, MNRAS, 357, 275
- King A.R., Ritter H., 1998, MNRAS, 293, L42
- Lasota J.-P., Alexander T., Dubus G., Barret D., Farrell S.A., Gehrels N., Godet O., Webb N.A., 2011, ApJ, 735, 89
- Leitherer C., et al., 1999, ApJS, 123, 3
- Lützgendorf N., Kissler-Patig M., Noyola E., Jalali B., de Zeeuw P.T., Gebhardt K., Baumgardt H., 2011, A&A, 533, 36
- Massey P., DeGioia-Eastwood K., Waterhouse E., 2001, AJ, 121, 1050
- Nonino M., et al., 2009, ApJSS, 183, 244
- O’Leary R.M., Loeb A., 2009, MNRAS, 395, 7810
- Peng C.Y., Ho L.C., Impey C.D., Rix H.-W., 2002, AJ, 124, 266
- Peng C.Y., Ho L.C., Impey C.D., Rix H.-W., 2010, AJ, 139, 2097
- Pickles A.J., 1998, PASP, 110, 863
- Pizzolato F., Wolter A., Trinchieri G., 2010, MNRAS, 406, 1116
- Portegies Zwart S.F., McMillan S.L.W., 2002, ApJ, 576, 899
- Schlegel D.J., Finkbeiner D.P., Davis M., 1998, ApJ, 500, 525
- Servillat M., Farrell S.A., Lin D., Godet O., Barret D., Webb N., 2011, ApJ, to appear in the 2011 December 10 issue (arXiv:1108.4405)
- Shakura N.I., Sunyaev R.A., 1973, A&A, 24, 337
- Soria R., Hau G.K.T., Graham A.W., Kong A.K.H., Kuin N.P.M., Li I.-H., Liu J.-F., Wu K., 2010, MNRAS, 405, 870
- Swartz D.A., Ghosh K.K., Tennant A.F., Wu K., 2004, ApJS, 154, 519
- Swartz D.A., Soria R., Tennant A.F., Yukita M., 2011, ApJ, 741, 49
- van der Marel R.P., Anderson J., 2010, ApJ, 710, 1063
- Vázquez G.A., Leitherer C., 2005, ApJ, 621, 695
- Vrtilek S.D., Raymond J.C., Garcia M.R., Verbunt F., Hasinger G., Kurster M. 1990, A&A, 235, 162
- Walton D.J., Roberts T.P., Mateos S., Heard V., 2011, MNRAS, 416, 1844
- Wiersema K., Farrell S.A., Webb N.A., Servillat M., Maccarone T.J., Barret D., Godet O., 2010, ApJ, 721, L102
- Worthey G., 1994, ApJS, 95, 107